Optical and Quantum Electronics (2023) 55:156
https://doi.org/10.1007/s11082-022-04434-9

Pt/PbSe optoelectronic receivers designed for 6G and terahertz communication technologies

Manal M. Alkhamisi[1] · A. F. Qasrawi[2,4] · Hazem K. Khanfar[3] · Sabah E. Algarni[5]

Received: 17 September 2022 / Accepted: 25 November 2022

Abstract
Herein PbSe thin films are coated onto glass and semitransparent platinum substrates. The films which are treated as optoelectronic signal receivers are deposited by the thermal evaporation technique under a vacuum pressure of 10^{-5} mbar. The structural investigations have shown that (glass, Pt)/PbSe films are of polycrystalline nature. Optically, Pt substrates increased the transparency and reflectivity of PbSe films. The energy band gap of PbSe is also increased by 0.12 eV when films are coated onto Pt substrates. In addition the dielectric constant also increased as a result of strong interaction between Pt plasmonic particles and lead selenide. On the other hand, fitting of the imaginary part of the dielectric constant using Drude–Lorentz model has shown that coating of PbSe onto semitransparent Pt substrates increased the drift mobility of lead selenide by four times. Pt substrates resulted in a decrease in the density of free charge carriers and increases the scattering time constant at femtosecond levels. (Glass, Pt)/PbSe optoelectronic receivers displayed plasmon frequencies up to ~ 13 GHz and showed terahertz cutoff frequency of ~ 1.0 THz. In addition, allowing the propagation of an ac signal of low amplitude in the Pt/PbSe/Pt receivers has shown that the devices exhibit wide range of resistance tunability. The microwave cutoff frequency also reached 14 GHz. Both of the optical and electrical measurements proved the suitability of the Pt/PbSe devices for 6G and terahertz communication technologies.

Keywords PbSe · Thermal evaporation · Negative capacitance · Microwave · 6G technology

✉ A. F. Qasrawi
atef.qasrawi@aaup.edu; atef.qasrawi@istinye.edu.tr

[1] Department of Physics, College of Science and Art, King Abdulaziz University, Rabigh, Saudi Arabia

[2] Department of Physics, Arab American University, Jenin, Palestine

[3] Department of Telecommunication Engineering, Arab American University, Jenin 240, Palestine

[4] Department of Electrical and Electronics Engineering, Istinye University, 34010 Istanbul, Turkey

[5] Department of Physics, Faculty of Science, University of Jeddah, Jeddah, Saudi Arabia

Published online: 30 December 2022

1 Introduction

PbSe thin films have attracted the attention of researchers due to their wide range of applications in communication technology. As for examples, lead selenide-bismuth selenide heterojunctions displayed features of high sensitivity and fast response infrared detectors (Ren et al. 2022). These detectors revealed a current responsivity of 31.4 A/W and showed high IR detectivity up to 1.7×10^{11} cmHz$^{1/2}$/W (Ren et al. 2022). In another work PbSe was used in the design of GeSe/PbSe infrared photoinverter showing a detectivity of 5.8×10^{14} jones and responsivity of 1.26 V×10^6/W (Liu et al. 2022). These devices were found suitable for applications in spectroscopy and for quick chemical gas sensing (Liu et al. 2022). In addition, PbSe targets have nuclear applications (Chiera et al. 2022). It is employed for ^{79}Se neutron capture cross section studies.

PbSe thin films are coated onto metal and semiconductor substrates. The nature of the substrate strongly alters the properties and performance of the lead selenide films. It is mentioned that thin films of lead selenide coated onto GaAs substrates undergo in-plane tensile strain which increases the energy band gap by 10% (Liu et al. 2021). In addition, *n* -type PbSe thin films deposited onto *p*-type Ge substrates resulted in formation of crack -free monocrystalline lead selenide films (McDowell et al. 2022). Ge/PbSe structures demonstrated a strong *pn* diodes behavior with high rectifying factor and low reverse bias current density nominating it for use as photodetectors and other heterojunction applications (McDowell et al. 2022).

The sensitivity of the grown PbSe films to the substrate nature motivated us to deposit these films onto semitransparent Pt substrates. Our recent studies on SeO_2 thin films coated onto Pt semitransparent substrates have shown that Pt does not alter the structure of the SeO_2 films but increases the light absorbability by 50 times and enhanced the dielectric performance of selenium oxide (Alfhaid and Qasrawi 2022). The plasmon frequency of the Pt/SeO_2 films reached 6.0 GHz. For these reasons, here in this work, we are motivated to study the optoelectronic properties of the Pt/PbSe films in an attempt to find new class of applications of lead selenide in optoelectronic technology. One of these optoelectronic technology components is the optoelectronic signal receiver. Optoelectronic signal receiver is a device that extracts the baseband signal from a modulated optical carrier signal by converting incident optical power into electric current. In the current work lead selenide thin films will be coated onto glass and Pt substrates. The structural, morphological, compositional, optical, dielectric and impedance spectroscopy analyses will be carried out to explore the effect of Pt substrates on the properties of the films. Based on the experimental measurements the microwave and terahertz cutoff frequency spectra resulting from incident electromagnetic spectrum are calculated and discussed. Possible applications of the lead selenide thin films in 6G and terahertz communication technology as optoelectronic optical receivers will be suggested for the first time.

2 Experimental details

The source material for evaporating lead selenide thin films was PbSe crystals which are produced by the pulsed laser welding technique. The source material was welded in an argon atmosphere by mixing 0.25 g of high purity Se (99.999% Alpha-Aeser) with 0.25 g of high purity Pb (99.999%, Alpha Aeser) powders. The mixture was milled in a ball mill revolving at 50 rev/s for 5 min. After that the mixed powders were exposed to laser

irradiation. The pulsed pumping of laser light continued for ~ 2.0 min. The optimum pulse width was 50 ms. A laser light of wavelengths of 1064 nm was generated from IWELD 940 laser system. The resulting crystals were then situated in a quartz tube surrounded by a wounded tungsten coil and inserted into A NORM VCM -600 thermal evaporator. The glass which is used as substrates to coat Pt and PbSe was ultrasonically and chemically cleaned. Pt films of thicknesses of 100 nm were prepared by the ion coating technique from high purity Pt (99.999%) disks. The films were evaporated at a vacuum pressure of 10^{-5} mbar. The produced films thicknesses were determined by a profilometer working in the range of 5 nm–100 μm. The produced films are characterized by a X-ray diffraction unit (Miniflex 600) and COXEM 200 microscope equipped with EDAX energy dispersive X-ray analyzer. Pt was also used as point contact for the PbSe samples. The optical spectroscopy of the films was recorded by Evolution 300 spectrophotometer. The impedance spectroscopy was recorded with the help of Agilent 4291B 0.01–1.80 GHz impedance analyzer.

3 Results and discussion

Thin films of lead selenide (500 nm) are coated onto glass and semitransparent Pt substrates of thicknesses of 100 nm. For these films the X-ray diffraction patterns are illustrated in Fig. 1. The figure contained sharp patterns indicating the polycrystalline nature of the films. It is evident from the figure that the most intensive peak which appeared at diffraction angles of $2\theta = 29.55^{\circ}$ for glass/PbSe is shifted to $2\theta = 29.45^{\circ}$ when the same films

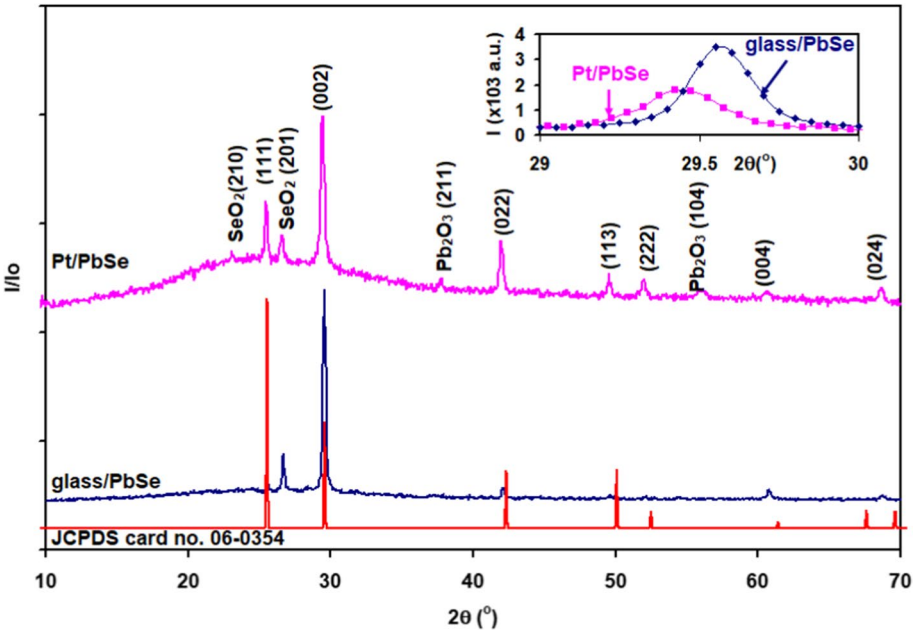

Fig. 1 X-ray diffraction patterns for lead selenide films deposited onto glass and semitransparent Pt substrates. The inset showing the enlargement of the most intensive peak

are coated onto pt substrates. In order to understand the crystallinity of the films, deep analyses using "Crystdiff" software packages were carried out. In accordance with the standard powder diffraction data for cubic PbSe (lattice parameters are a = b = c = 6.076 Å and symmetry space group of $F4m3m$ (225)) the most intensive peak of 100% relative intensity should appear at a diffraction angle of $2\theta = 25.38^{\circ}$. However for our grown films the most intensive peak revealing 100% appeared at of$2\theta = 29.55^{\circ}$. Compared to the to the JCPDS card no. 06-0354 which is shown in the same figure, the preferred plane orientation is along the (002) direction with diffraction angles of$2\theta = 29.55^{\circ}$. The calculated lattice parameter for this unit cell is 6.0336 Å. This nature of growth of the films was previously observed for PbSe in nanoparticle forms (Fu et al. 2012). In addition, as can be seen from the inset of Fig. 1, coating PbSe films onto Pt substrates shifted the diffraction angles toward lower diffraction angles and decreased the maximum peak intensity. For the Pt/PbSe films the lattice constant is 6.0636 Å. On the other hand as an important point of consideration, the hexagonal phase (Ghobadi et al. 2018; Wang et al. 2019; Borren 2014) of lead selenide (a = b = 3.505 Å, c=5.664 Å, space group: $P_{63/mmc}$ (194)) should display the maximum peak at diffraction angles of $2\theta = 29.40^{\circ}$ with planes oriented along (002) direction. Thus it is possible to think that the resulting crystal structure is hexagonal which sharp diffraction patterns appearing at diffraction angles of $2\theta = 29.30^{\circ}$,31.54°,43.59°,52.15°,61.00°,62.17° ,65.79°, 70.37° and73.85°, with plane oriented along (010), (002), (012), (110), (020), (112), (004), (022), (014), respectively. The peaks of the hexagonal phase which are found in our experimental data are$2\theta = 29.40^{\circ}$, 52.17° and 61.00°. However, as the same peaks appear in the cubic phase of PbSe then there is no way to decide whether the appearing three XRD patterns are from cubic or hexagonal planes. However, as the hexagonal phase of lead selenide is rarely observed and the strong reflection planes along (002) direction appearing at at $2\theta = 29.55^{\circ}$ are previously assigned to cubic phase of lead selenide (Fu et al. 2012; Bhat et al. 2017) in the following text parts we will assume that the structure is cubic.

It is also evident from Fig. 1 that a one minor peak which is detected at diffraction angles of $2\theta = 26.76^{\circ}$ relates to tetragonal SeO_2 (a=b=8.713 Å , c=5.203 Å space group: $P4_2/mbc$). The calculated phase weights ($\Delta\% = \sum 100.A_{phase}/\sum A_{allpeaks}$ A area of the peak (Qasrawi and Abu Ghannam 2022)) of the cubic PbSe and tetragonal SeO_2 were found be 88.64% and 11.36%, respectively. For the samples coated onto Pt substrates other minor peaks which were assignable to monoclinic Pb_2O_3 (JCPDS File No.89-7387) were observed. The lattice parameters for monoclinic Pb_2O_3 are a=5.762 Å , b=7.700 Å, c=7.974 Å, , $\alpha = 67.089^{\circ}$ and space group: $P2_1c$ (14). The phase weights of cubic PbSe, tetragonal SeO_2 and monoclinic Pb_2O_3 in Pt/PbSe films are 89.69%, 7.00% and 3.31%, respectively. The data suggest that Pt substrates induced the formation of Pb_2O_3 without significant effect on the phase weight of cubic PbSe.

It can be seen from the inset shown in Fig. 1 that the maximum peaks of the recorded XRD patterns is shifted and the intensity is decreased when the PbSe films are deposited onto transparent Pt substrates. The shifts and peak broadenings are indicators of possible strain induced structural deformations resulting from the interaction between Pt plasmonic layers and PbSe (Nasiri-Tabrizi 2014). Strong non-uniform strain is mentioned developing within the domain of electron–phonon interaction time (Plech et al. 2004). In this process delocalized plasmon resonance extending over several adjacent particles can result in a shift of the diffraction patterns due to the shortening of the average distance between the interacted particles. The shorter distance enhances the coupling field between the interacted particles (Plech et al. 2004). On the other hand benefiting from maximum peak broadening (β) at full wave half maximum we have calculated the structural parameters. The structural parameters presented by the lattice constant (a), the crystallite sizes

($D = \frac{0.94\lambda}{\beta cos\theta}$ (Qasrawi and Abu Ghannam 2022)), the strain ($\in = \frac{\beta}{4tan\theta}$, the staking faults ($SF\% = \frac{2\pi^2\beta}{45\sqrt{3}\tan(\theta)}$ (Qasrawi and Abu Ghannam 2022)) and the defects density ($\delta = \frac{15\in}{aD}$ (Qasrawi and Abu Ghannam 2022)) are calculated and listed in Table 1. In accordance with the table, the lattice constant, the microstrain, the stacking faults and the defects density increases while the crystallite sizes decreases when PbSe films is coated onto Pt substrates instead of glass. The lattice constant increases because of the interstitial substitutions of Pt ions in sites of Pb and Se (Mustafa et al. 2022). Since the ionic radii of Pt^{+2} being 80–96 pm (Xu et al. 2019; Levy et al. 2007) is larger than that of Pb^{+4} (0.78 Å (Qasrawi and Abu Ghannam 2022)) and larger than that of Se^{+4} (0.64 Å (Nasiri-Tabrizi, 2014)) it may lead to an increase in the lattice constant and in the defect density (Mustafa et al. 2022; Qasrawi 2022). In addition, the decrease in the crystallite sizes which resulted from coating PbSe onto Pt substrates probably resulted in an overall increased rates of electron–phonon scattering due to spatial confinement of electrons, phonons and their additional scattering with defects and grain boundaries (one grain is an accumulation of group of crystallites) (Sharma and Okram 2019). Moreover interaction of Pt ions with PbSe and performing of these interacted particles as doping agents leads to an increased impurity concentration. Hence the average crystallite size decreases because of the strain induced in the cubic lattice of PbSe (Paulson et al. 2019).

Figure 2 illustrates the results of the scanning electron microscopy (SEM) and energy dispersive X-ray (EDS) measurements of the PbSe films coated onto glass and Pt semi-transparent substrates. As can be seen from Fig. 2a and its inset very small grains are distributed at two levels through the glass/PbSe film. The grains appearing as white dots are grains of average sizes of 100 nm and the hardly seen grains are of smaller sizes (~ 50 nm). Inset 1 of Fig. 2b shows the SEM images for Pt plasmonic particles before coating of PbSe. Randomly distributed grains of irregular shapes and of average sizes of 350 nm can be observed (red circles in inset-1 of Fig. 2b). Coating Pt nanosheets with PbSe resulted in the images shown in Fig. 2c. Black circular regions (clusters) of average diameter of 1.5 μm can be observed (green circles). When the image is enlarged further (Inset-2 of Fig. 2b) one may see other tiny circular black regions or clusters (blue circles) randomly distributed in the surrounding regions of larger black circles (clusters). The average diameter of these tiny black regions are ~ 450 nm. Comparing the Pt substrates with the Pt/PbSe films we observed that the formation of black regions of large and small sizes depends on the size of the Pt particles. Other regions where circular black regions were not observed (shown by rectangular shaped region) displayed very dense grain distribution of sizes of 90 nm.

On the other hand, the energy dispersive X-ray spectra for the glass/PbSe and Pt/PbSe film are shown in Fig. 2b. As seen from the spectra, the films are composed of glass ($SiO:Na_2O:MgO:CaO$), Pb, Se, Pt and Au only. No other impurities were detected in the films. Au existed because glass/PbSe films were coated with Au to prevent electron contamination at the surface. Samples coated onto Pt were not coated with Au to allow distribution of Pt from Au and due to the higher conductivity of the Pt/PbSe films compared

Table 1 The structural parameters for glass/PbSe and Pt/PbSe thin films

Sample	a Å	D (nm)	$\epsilon \times 10^{-3}$	SF%	$\delta(\times 10^{11}\text{lines}/cm^2)$
Glass/PbSe	6.0336	41	3.47	0.18	2.10
Pt/PbSe	6.0636	34	4.23	0.22	3.08

to glass/PbSe. The numerical analyses of the EDS spectra over many samples and different scanning areas of studied samples have shown that glass/PbSe and Pt/PbSe films are composed of 38.56 at. % Pb and 61.44 at. % Se and 65.68 at. % Se and 34.32 at. % Pb, respectively. For glass/PbSe and Pt/PbSe films the chemical formulas of lead selenide are $PbSe_{1.59}$ and $PbSe_{1.91}$, respectively. The large and tiny black circles revealed the chemical formulas $PbSe_{1.64}$ and $PbSe_{1.5}$, respectively. In other words, while films coated onto glass have tendencies to form Pb_2Se_3 phase which can be treated a mixture of PbSe and $PbSe_2$, those coated onto Pt forms selenium deficient $PbSe_2$. We can conclude that the black circular grains are relating to Pb_2Se_3 phase of lead selenide and the other remaining regions is composed of $PbSe_2$. This result is also consistent with our XRD analyses which revealed a decrease in the phase weight of SeO_2 (form 11.36% for glass/PbSe to 7.00% for Pt/PbSe) when films were coated onto Pt substrates. The dramatically changing chemical stoichiometry of the samples from Pb_2Se_3 (a mixture of PbSe and $PbSe_2$) to $PbSe_2$ in the presence of Pt can be assigned to the dissociation of PbSe into Pb and Se at lower energy (302 kJ/mol) compared to SeO_2 (464 kJ/mol) and Pb_2O_3 (382 kJ/mol) (Yan et al. 2020). Broken-bonds of Pb and Se have strong tendency to interact with oxygen when films are exposed to air because of the need for thermodynamic stability which is satisfied through breaking of Pb–Se and formation of Se–O and Pb–O (Yan et al. 2020; Pellissier et al. 2007). In addition from chemical point of view, when films are coated onto Pt substrates the content of Pb decreased and the content of Se increased (mostly PbSe become absent or accumulated in the black colored grains and $PbSe_2$ remained). Initially as the bond length of Se–O (1.64 Å (Alfhaid and Qasrawi 2022)) is shorter than that Pb–O (2.318 Å (Qasrawi and Abu Ghannam 2019)) and of Pb–Se (3.11 Å (Mao et al. 2022)), due to its abundance in the structure, broken bonds of Se interact with O resulting in formation of SeO_2. Then, as the bond the length of Pt–Se being 2.53 Å (Alfhaid and Qasrawi 2022) which is shorter than that of Pb–Se, some weakly bonded Se atoms interact with Pt to form PtSe leaving Pb atoms un-bonded. Because Pb–O has shorter bond length than lead selenide broken bonds of Pb interact with oxygen to form lead oxide (observed in XRD analyses).

Figure 3a and b illustrates the optical transmittance (T%) and reflectance (R%) spectra for PbSe thin films coated onto glass and semitransparent Pt substrates. The inset of Fig. 3a show the transmittance spectra of the Pt film. The transmittance of the platinum films increases from 59 to 63% as the incident light energy decreases from 2.5 to 1.14 eV. It means that the Pt films are sufficiently transparent allowing optical interaction at the Pt/PbSe films easily. Pt substrates also show a constant reflectance of ~ 10–11% in the studied incident photon range. It is also clear from Fig. 3a and b that the transmittance and reflectance of glass/PbSe films increases when Pt nanosheets are inserted between glass and PbSe films. The increase in the transmittance is probably due to the formation of lead oxide at the surface of the Pt/PbSe films. It was observed that formation of silver oxide in Ag films increases the optical transmittance (Hajakbari and Ensandoust 2016). Suppression of surface plasmon resonance and destructive interference of reflected light from the interface and from the surface could also accounts for the increased optical transmittance (Choi et al. 2020). In addition, the absorption coefficient (α) is calculated from the optical transmittance and reflectance using the relation (Alfhaid and Qasrawi 2022),

$$T \approx \left(1 - R_{glass}\right)\left(1 - R_{Pt}\right)\left(1 - R_{Pt/PbSe}\right)\exp(-\alpha d) \quad (1)$$

With d being the film thickness. When using Eq. (1) to find the absorption coefficient of glass/PbSe films, $R_{pt} = 0$ is substituted. As seen from Fig. 3c the absorption

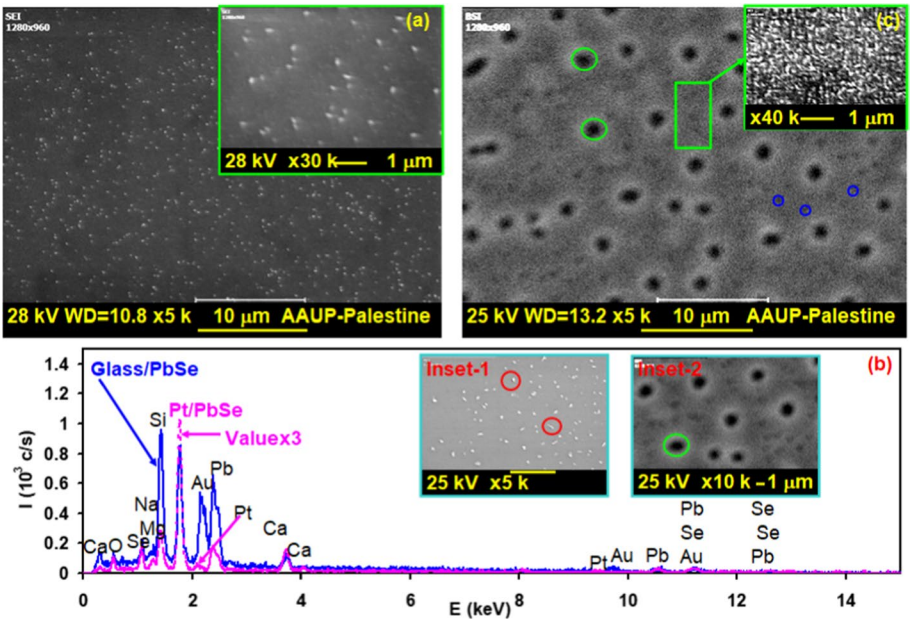

Fig. 2 **a** The scanning electron microscopy (SEM) images for **a** glass/PbSe and **b** Pt/PbSe films. **c** The energy dispersive X-ray spectra for glass/PbSe and Pty/PbSe films. Inset of **a** and inset of **b** showing the enlargements by 30,000 and 40,000 times for the glass/PbSe and Pt/PbSe films, respectively. Inset-1 of **c** displaying the SEM images for Pt and Pt/PbSe films, respectively

coefficient spectra exhibit absorption saturation in the spectral range of 2.50–1.65 eV and 2.50–2.10 eV when PbSe is coated onto glass and Pt substrates, respectively. The absorption saturation results from the carrier scattering into regions of lower mobility (Hebling et al. 2009) Moreover, it is believed that light of energy higher than the band gap of the material excites the free charge carriers to states of higher energy in the initial conduction band valley (related to energy levels distribution in the momentum space which have Γ point as an origin in the first Brillouin zone of cubic PbSe) from which they may scatter into other side valleys (Hebling et al. 2009). It is also observed from the absorption spectra of the studied films (Fig. 3c) that coating PbSe films onto Pt substrates remarkably decreased the absorption coefficient values and changed the shape of the $\alpha - E$ dependence. The absorption level decreases probably due to an increase in the energy band gap as a result of using Pt substrates (Park et al. 2021). This judgment can be confirmed by employing Tauc' equation ($(\alpha E)^{1/2} \propto (E - E_g)$) for indirect allowed transitions (most appropriate equation which linearized most of the optical data) (Alfhaid and Qasrawi 2022). The Tauc's equation fitting of the $(\alpha E)^{1/2} - E$ variations which are illustrated in Fig. 3d reveal an energy band gap of 0.50 eV and 0.62 eV for glass/PbSe and Pt/PbSe films, respectively. A blue shift by 0.12 eV is observed upon replacement of glass by Pt substrates. Hence the lowered absorption level is attributed to the increased energy band gap values of PbSe. The band gap increases due to the decrease in the crystallite sizes an increase in the microstrain (Agrahari et al. 2016; Tiwari et al. 2018). Our XRD analyses have shown that Pt substrates lead to a decrease in the crystallite size and increase in the microstrain from 41 to 34 nm and from 3.47×10^{-3} to 4.23×10^{-3}, respectively upon replacement of glass by Pt film. The

value of the optimized energy band gap of lead selenide being 0.50 eV is comparable to the value being 0.43 eV which is computed for cubic structure of lead selenide (Persson 2014).

To reveal information about the effects of Pt nanosheets on the dielectric spectra of lead selenide, the real (ε_r) and imaginary (ε_{im}) parts of the dielectric spectra were calculated and shown in Fig. 4a and (b), respectively. The effective dielectric spectra (ε_{eff}) are calculated from the reflectance and absorption coefficient spectra using Fresnel's equations (Alfhaid and Qasrawi 2022),

$$R = \frac{\left(\sqrt{\varepsilon_{eff}} - 1\right)^2 + (\alpha\lambda/(4\pi))^2}{\left(\sqrt{\varepsilon_{eff}} + 1\right)^2 + (\alpha\lambda/(4\pi))^2} \tag{2}$$

$$\varepsilon_r = \varepsilon_{eff} - (\alpha\lambda/(4\pi))^2 \tag{3}$$

and

$$\varepsilon_{im} = 2\sqrt{\varepsilon_{eff}}.\alpha\lambda/(4\pi). \tag{4}$$

In accordance with the spectra shown in Fig. 4a the dielectric constant values increased when films are coated onto Pt substrates. Enhancement of the dielectric spectra upon using Pt substrates was previously observed for Pt/SeO_2 thin films (Alfhaid and Qasrawi 2022). The enhancement in the dielectric spectra was assigned to the strong plasmonic interactions at the Pt/SeO_2 interfaces (Alfhaid and Qasrawi 2022). The increase in the dielectric

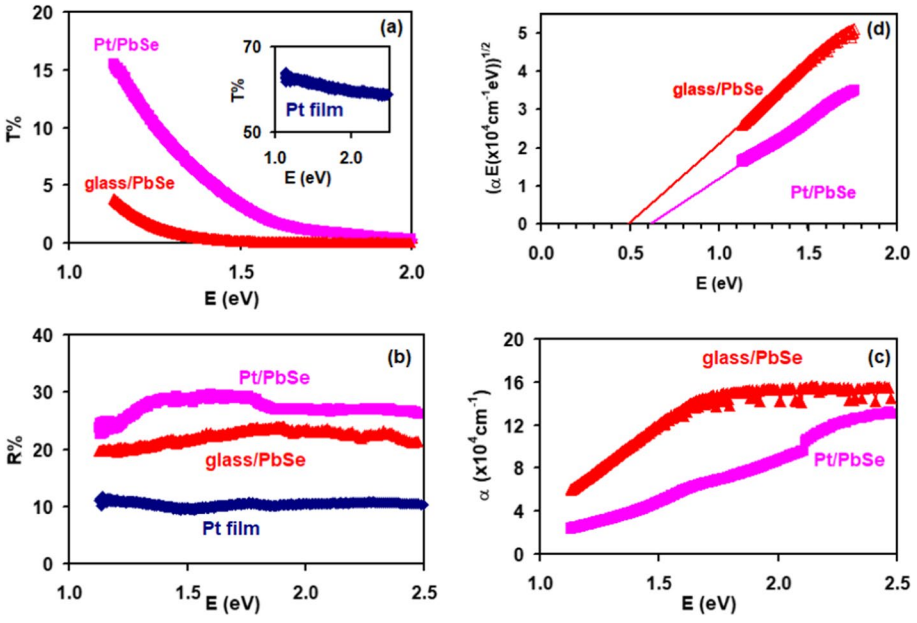

Fig. 3 **a** The transmittance, **b** the reflectance, **c** the absorption coefficient spectra for PbSe films coated onto glass and Pt substrates and **d** the Tauc's equation fittings for the studied films

constant can also be assigned to the combined effect of Maxwell–Wagner effect and spontaneous polarization arising due to local dipole moment (Virpal et al. 2017). Maxwell–Wagner effects accounts for charge accumulation at the Pt/PbSe interface on the basis of the difference of charge carrier relaxation times in these two materials (Pt and PbSe). Spontaneous polarization plays role under the influence of internal process in a dielectric media in the absence of external factors. On the other hand, the imaginary part of the dielectric spectra displayed in Fig. 4b show an opposite behavior to that of the real part. Namely, coating PbSe onto Pt substrates remarkably decreased the values of the imaginary part. While ε_{im} spectra of glass/PbSe show a maxima at 1.71 eV, the maxima are suppressed and become broaden when PbSe films are coated onto Pt substrates. The observed maxima at 1.71 eV can be attributed to the transitions from the highest occupied molecular orbitals (HOMO) centered at ($1e_{3/2}$) to the lowest unoccupied molecular orbitals (LUMO) centered at ($4e_{1/2}$) molecular states of the $(PbSe)_1$ clusters (Zeng et al. 2013). Possible formation of clusters was observed though our SEM analyses. Molecular dynamics studies have shown that two growth patterns with distinct structures and energy evolutions are guessed for even and odd clusters ($(PbSe)_n$, n is number of low laying structure) (Zeng et al. 2013). These clusters grow in simple cubic and bulk like growth patterns (very similar to the black large and small regions we observed through SEM studies (Fig. 2)). It is mentioned that the orbital overlapping between 6*p* of lead and 4*p* of selenium make stable building blocks of $(PbSe)_4$ with ordered and bulk like structures. $(PbSe)_4$ reveals larger size clusters (Zeng et al. 2013).

Reproducing the imaginary part spectra of the glass/PbSe and Pt/PbSe films using Drude-Lorentz approach it was possible to obtain information about these HOMO-LUMO transitions and about the optical conductivity parameters. Drude–Lorentz model defines the imaginary part of the dielectric spectra by the equations,

$$\varepsilon_{im} = \sum_{i=1}^{k} \frac{w_{pi}^2 w}{\tau_i \left(\left(w_{ei}^2 - w^2 \right)^2 + w^2 \tau_i^2 \right)}, \tag{5}$$

$$w_{pe} = \sqrt{4\pi P\, e^2/m^*} \tag{6}$$

$$\tau_i = \mu_i m^*/e. \tag{7}$$

with w_{pe} being plasmon frequency, τ_i is the average scattering time at femtosecond level, W_{ei} is the hole-plasmon coupled oscillator frequency, P is the free hole density and μ is the drift mobility.

The fitting of the experimental data which is shown by blue colored circles in Fig. 4b was possible by running the series of Eq. (5) up to $k = 4$ and assuming the fitting parameters shown in Table 2.The reduced effective mass for Pt/PbSe ($m^*_{Pt/PbSe} = \left(m^{*^{-1}}_{Pt} + m^{*^{-1}}_{PbSe} \right)^{-1}$) was calculated assuming electron effective mass of $m^*_{Pt} = 1.0 m_o$ (Alfhaid and Qasrawi 2022; Ge et al. 2011) and holes effective mass of m^*_{PbSe}=0.17 m_o (Mao et al. 2022).

In accordance with Table 2, the optical conductivity ($\sigma(w) = \varepsilon_{im} w/(4\pi)$; w radial frequency) parameters for glass/PbSe films are defined by oscillators of energies of 1.31 eV, 1.71 eV, 1.90 eV and 2.98 eV. The oscillator energy being 1.71 eV is originated from the HOMO-LUMO transitions through $(PbSe)_1$ clusters (Ge et al. 2011). The value of the oscillator energy being 1.90 eV originates from excitations in $(PbSe)_1$ clusters with

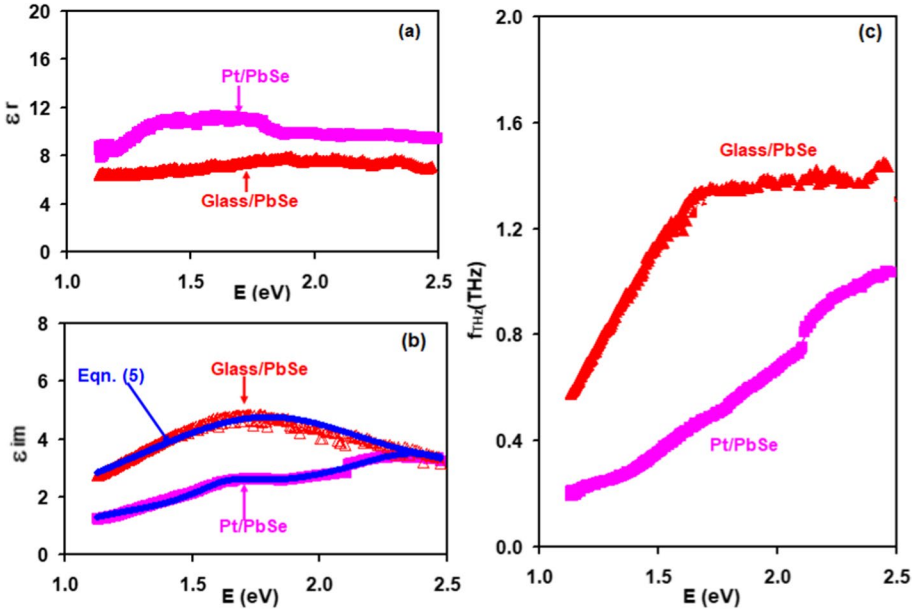

Fig. 4 **a** The real, **b** the imaginary parts of the dielectric spectra and **c** the terahertz cutoff frequency spectra for glass/PbSe and Pt/PbSe thin films

first excitation appearing at 1.90 eV with spin forbidden transitions from HOMO (1π) to LUMO (2π) molecular states. The oscillator energy being 2.98 eV is related to exciton transitions within (1π) molecular states of $(PbSe)_1$. It is also observed that a redshift in the oscillators energy from 1.31 to 1.18 eV, 1.71 to 1.64 eV and from 2.98 to 2.43 eV is observed when Pt replaces glass. The oscillator energy values being 1.64 eV, 1.90 eV and 2.43 eV correspond to molecular transitions within$S-S$; $1(1A_2)$ of $(PbSe)_2$,$S-T$; $1(1\sum^{+})$ of $(PbSe)_1$ and $S-T$;$1(1A_1)$ of $(PbSe)_4$ clusters (Ge et al. 2011), respectively. The value of the oscillator energy being 1.31 eV is very close to that observed as 1.29 eV for HOMO-LUMO$S-S1(1A_1)$ transitions within $(PbSe)_3$ clusters. In addition, the critical energy value detected at 1.18 eV corresponds to indirect optical transitions within the energy band gap of $PtSe_2$ (Sajjad et al. 2018; Guo 2016). In the structural investigations we have mentioned that interaction between Pt and Se is preferred over Pt–Se owing to the shorter bond length of the latter (Alfhaid and Qasrawi 2022).

As also can be seen from Table 2, the free hole density decreased by 10 times for the infrared oscillators (1.18 eV, 1.64 eV) and by ~ 2 times for the visible light oscillators (1.90 eV, 2.43 eV). This decrease in the free carrier density increased the scattering time constant and forced the drift mobility to exhibit higher values. The highest achievable drift mobility is 22.44 cm^2/Vs for free charged carriers propagating under the influence of electromagnetic fields within distances of ~ 500 nm. Literature data reported mobility values of 7.0 cm^2/Vs for PbSe quantum dots thin films prepared via in-solution ligand exchange (Nakotte et al. 2020) method. A higher value of mobility (16 cm^2/Vs) is obtained via annealing the films at 300 °C (Yan et al. 2020). The data shown in Table -2 indicate that coating PbSe onto transparent Pt substrate is a novel method to enhance the mobility values of PbSe.

Table 2 Optical conductivity parameters for glass/PbSe and Pt/PbSe films computed by Drude-Lorentz approach

	Glass/PbSe				Pt/PbSe			
i	1	2	3	4	1	2	3	4
E_e (eV)	1.31	1.71	1.90	2.98	1.18	1.64	1.90	2.43
τ (fs)	0.5	0.5	0.5	0.5	1.5	2.0	0.4	0.8
p ($\times 10^{18}$ cm^{-3})	10.0	28.0	70.0	80.0	0.9	2.6	43.0	44.0
ωp (GHz)	4.56	7.62	12.06	12.89	1.42	2.42	9.84	9.96
μ (cm^2/Vs)	5.17	5.17	5.17	5.17	16.83	22.44	4.49	8.98

Another remarkable point which can be observed from Table 2 is that the plasmon frequency values of glass/PbSe and Pt/PbSe are high enough to nominate the currently studied interfaces for communication technologies including 6G technology (Alfhaid and Qasrawi 2022; F. Carvalho and Mejía-Salazar, 2020; Qasrawi and Sulaiman 2022). Further information about the applications of these metal/semiconductor layers in communication technology can be found from the terahertz cutoff frequency spectra ($f_{THz} = \varepsilon_{im} w/(4\pi\varepsilon_r)$ which are shown in Fig. 4c. The terahertz cutoff frequency is defined as the frequency at which energy flowing through the system begins to be attenuated (reflected or reduced) rather than passing through (Alfhaid and Qasrawi 2022). In an optoelectronic system like band filters and communication channels the cutoff frequency applies to an edge in a low-pass, highpass, bandpass, or band-stop characteristic curves. It is a frequency characterizing a boundary between a passband and a stopband. In the case of a waveguide or an antenna, the cutoff frequencies correspond to the lower and upper cutoff wavelengths. As seen from Fig. 4c based on the exciting electromagnetic field energy (incident light energy) one my identify the cutoff point of the propagating signals. Wider tunability of f_{THz} is achieved for Pt/PbSe films especially in the visible range of light. Since the highest cutoff frequency leads to the highest efficiency of the optoelectronic devices used in communication technology, obtaining values larger than 1.0 THz is accounted as a smart property for terahertz applications (Zimmermann et al. 1995).

To verify the validly of the plasmon frequency as a cutoff limit suitable for 6G technologies we have imposed a Pt/PbSe/Pt device between the terminals of an impedance analyzer providing ac signals of waveform. The amplitude of the signal was kept low (0.10 V). The resulting ac resistance (R), capacitance (C) and microwave cutoff frequency ($f_{co} = 1/(2\pi RC)$ (Alfhaid and Qasrawi 2022; Sze et al. 2021)) spectra are shown in Fig. 5a, b and c, respectively. It is clear from the Fig. 5a that the resistance sharply decreased with increasing ac signal frequency. A decay by more than two orders of magnitude can be observed. On the other hand, within the same frequency domain the capacitance slowly decreased with increasing signal frequency indicating that the devices are controlled by the resistive part rather than reactive part. The cutoff frequency increases (Fig. 5c) accordingly. It reaches values of ~ 12–14.0 GHz for ac signals of frequency of 1.0 GHz. This is the same value we observed from light signal analyses. Drude-Lorentz approaches showed plasmon frequency (cutoff) values reaching 12.89 GHz (Table 2). Hence the impedance spectroscopy analyses also show the possible application of the fabricated Pt/PbSe/Pt devices for 6G technology applications.

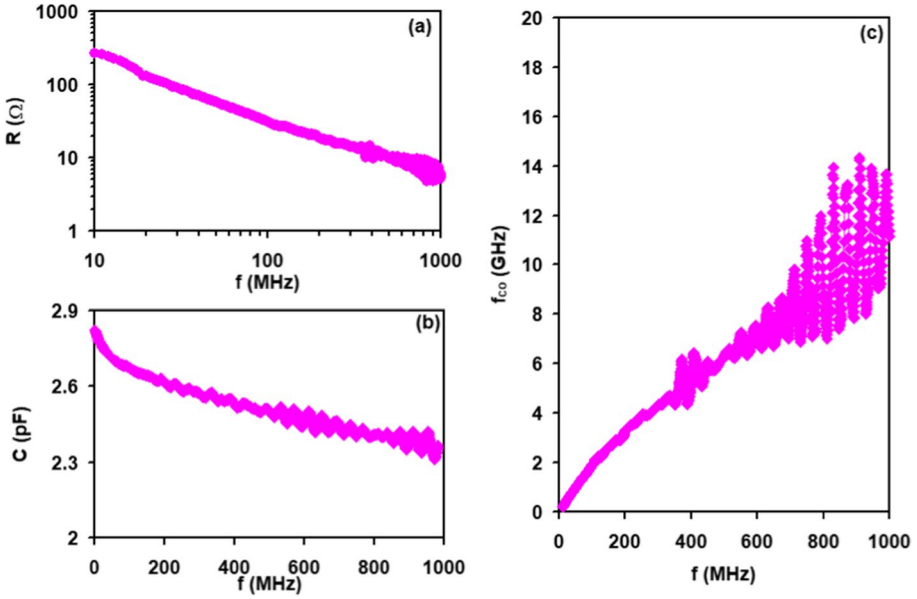

Fig. 5 **a** The resistance, **b** the capacitance and **c** the cutoff frequency spectra for Pt/PbSe/Pt devices

4 Conclusions

In this work we have shown that coating PbSe thin films onto semitransparent Pt substrates can significantly change the chemical stoichiometry of the films and changes the surface morphology of the films. Strong interactions between Pt and weakly bonded Se atoms caused formation of lead oxide in the films. One may also engineer the optical properties of lead selenide by Pt semitransparent substrates. The coupling between these two layers resulted in narrowing the energy band gap of PbSe which in turn led to an increment in the transmittance of the lead selenide films. Interactions between Pt and PbSe increased the drift mobility of the charge-carriers through the films making it more appropriate for opto-electronic applications. It is also observed that PbSe films exhibiting plasmon and cutoff frequency values larger than 12 GHz are suitable for 6G technology applications. The films are also found suitable for terahertz applications.

Acknowledgements The authors gratefully acknowledge the technical and financial supportprovided by the Ministry of Education and King Abdulaziz University,DSR, Jeddah, Saudi Arabia.h thanks DSR for technical.

Authors' contributions MMA wins the grand and together with SEA collected the optical data and determined values corresponding to Figs. 3 and 4. HKK prepared the optimum source material by laser welding technique. Qasrawi AF edited the article and determined the results based on Figs. 1, 2 and 5. He also carried out the Drude–Lorentz modeling to obtain data listed in Table 2. All authors reviewed the manuscript.

Funding This research work was funded by Institutional Fund Projects under grant no. IFPIP:0337-665-1443. The authors gratefully acknowledge the technical and financial support provided by the Ministry of Education and King Abdulaziz University, DSR, Jeddah, Saudi Arabia.

Data availability The data that support the findings of this study are available from the corresponding author upon reasonable request.

Declarations

Competing interests The authors declare that they have no conflict of interest.

References

Agrahari, V., Mathpal, M.C., Kumar, S., Kumar, M., Agarwal, A.: Cr modified Raman, optical band gap and magnetic properties of SnO_2 nanoparticles. J. Mater. Sci. Mater. Electron. **27**(6), 6020–6029 (2016)

Alfhaid, L.H.K., Qasrawi, A.F.: Pt/SeO_2 optical receivers designed for terahertz and 5G/6G technologies. Phys. Scr. **97**(5), 055820 (2022)

Bhat, T.S., Shinde, A.V., Devan, R.S., Teli, A.M., Ma, Y.R., Kim, J.H., et al.: Structural and electrochemical analysis of chemically synthesized microcubic architectured lead selenide thin films. Appl. Phys. A **124**(1), 34 (2017)

Borren, E.: I. Synthesis and reactivity of novel β-Diketiminato-cadmium complexes, II. Synthesis of lead selenide nanoparticles for use in solar cells. (2014)

Carvalho, W.O.F., Mejía-Salazar, J.R.: Plasmonics for telecommunications applications. Sensors **20**(9), 2488 (2020)

Chiera, N.M., Maugeri, E.A., Danilov, I., Balibrea-Correa, J., Domingo-Pardo, C., Köster, U., et al.: Preparation of PbSe targets for ^{79}Se neutron capture cross section studies. Nucl. Instrum. Methods Phys. Res. Sect. A **1029**, 166443 (2022)

Choi, D.-H., Seok, H.-J., Kim, D.-H., Kim, S.-K., Kim, H.-K.: Thermally-evaporated $C_{60}/Ag/C_{60}$ multilayer electrodes for semi-transparent perovskite photovoltaics and thin film heaters. Sci. Technol. Adv. Mater. **21**(1), 435–449 (2020)

Fu, H., Luan, W., Tu, S.-T.: A simple route for synthesis of PbSe nanocrystals: shape control by ligand and reaction time. Dalton Trans. **41**(39), 12254–12258 (2012)

Ge, C., Jin, K.-J., Wang, C., Lu, H.-B., Wang, C., Yang, G.-Z.: Numerical investigation into the switchable diode effect in metal-ferroelectric-metal structures. Appl. Phys. Lett. **99**(6), 063509 (2011)

Ghobadi, N., Sohrabi, P., Haidari, G., Haeri, S.S.H.: The effect of pH on the optical band gap of PbSe thin film with usability in the quantum dot solar cell and photocatalytic activity. J. Interfaces Thin Films Low Dimens. Syst. **2**(1), 139–147 (2018)

Guo, S.-D.: Biaxial strain tuned thermoelectric properties in monolayer $PtSe_2$. J. Mater. Chem. C **4**(39), 9366–9374 (2016)

Hajakbari, F., Ensandoust, M.: Study of thermal annealing effect on the properties of silver thin films prepared by DC magnetron sputtering. Acta Phys. Pol. A **129**(4), 680–682 (2016)

Hebling, J., Hoffmann, M. C., Hwang, H. Y., Yeh, K.-L., & Nelson, K. A. Nonlinear optical effects in germanium in the THz range: THz-pump—THz-probe measurement of carrier dynamics. Paper presented at the Ultrafast Phenomena XVI, Berlin, Heidelberg (2009)

Levy, C., Guizard, C., Julbe, A.: Soft-chemistry synthesis, characterization, and stabilization of CGO/Al_2O_3/Pt nanostructured composite powders. J. Am. Ceram. Soc. **90**(3), 942–949 (2007)

Liu, X., Wang, J., Riney, L., Bac, S.K., Smith, D.J., McCartney, M.R., et al.: Unraveling the structural and electronic properties of strained PbSe on GaAs. J. Cryst. Growth **570**, 126235 (2021)

Liu, X., Lin, H.X., Hang, Z.Y., Tang, Z.W., Liu, Z., Sun, J., et al.: An Infrared Photoinverter With a GeSe 2-D/PbSe Heterostructure and its application in spectroscopy detectors. IEEE Electron Device Lett. **43**(7), 1085–1088 (2022)

Mao, Y., Wu, R., Ding, D., He, F.: Tunable optoelectronic properties of two-dimensional PbSe by strain: first-principles study. Comput. Mater. Sci. **202**, 110957 (2022)

McDowell, L.L., Qiu, J., Mirzaei, M.R., Weng, B., Shi, Z.: Integration of epitaxial IV–VI Pb-Chalcogenide on group IV vicinal ge substrate to form p–n heterogeneous structures. Cryst. Growth Des. **22**(1), 461–468 (2022)

Mustafa, G., Khalid, M., Chandio, A.D., Shahzadi, K., Uddin, Z., Khan, J.K., et al.: Dielectric, impedance, and modulus spectroscopic studies of lanthanum-doped nickel spinel ferrites $NiLaxFe_2$–xO_4 nanoparticles. J. Sol-Gel. Sci. Technol. **101**(3), 596–605 (2022)

Nakotte, T., Luo, H., Pietryga, J.: Carrier density modulation in PbSe quantum dot films via in-solution ligand exchange. MRS Adv. **5**(40–41), 2091–2099 (2020)

Nasiri-Tabrizi, B.: Thermal treatment effect on structural features of mechano-synthesized fluorapatite-titania nanocomposite: a comparative study. J. Adv. Ceram. **3**(1), 31–42 (2014)

Park, S., Choi, S., Kim, S., Nam, K.T.: Metal halide perovskites for solar fuel production and photoreactions. J. Phys. Chem. Lett. **12**(34), 8292–8301 (2021)
Paulson, A., Muhammed Sabeer, N.A., Pradyumnan, P.P.: A synergetic approach of band gap engineering and reduced lattice thermal conductivity for the enhanced thermoelectric property in Dy ion doped ZnO. J. Alloy. Compd. **786**, 581–587 (2019)
Pellissier, A., Bretonnière, Y., Chatterton, N., Pécaut, J., Delangle, P., Mazzanti, M.: Relating structural and thermodynamic effects of the Pb(II) lone pair: a new picolinate ligand designed to accommodate the Pb(II) lone pair leads to high stability and selectivity. Inorg. Chem. **46**(9), 3714–3725 (2007)
Persson, K.: Materials data on PbSe (SG:225) by materials project. Accessed (2014)
Plech, A., Grésillon, S., von Plessen, G., Scheidt, K., Naylor, G.: Structural kinetics of laser-excited metal nanoparticles supported on a surface. Chem. Phys. **299**(2), 183–191 (2004)
Qasrawi, A.F.: Plasmonic interactions at the Pb/SeO_2 interfaces designed as terahertz/gigahertz optical receivers. Optik **265**, 169529 (2022)
Qasrawi, A.F., Abu Ghannam, A.N.: *In situ* monitoring of heat assisted oxidation and its effects on the structural, dielectric and optical conductivity parameters of Pb thin films as promising terahertz transmitters. Mater. Res. Express **6**(11), 116412 (2019)
Qasrawi, A.F., Abu Ghannam, A.N.: Optical and electrical dynamics at the In/CuSe interfaces. Optik **252**, 168505 (2022)
Qasrawi, A.F., Sulaiman, S.K.: Effects of SeO_2 epilayer on the structural, morphological, optical and dielectric properties of nanocrystalline ZnSe thin films. Physica B **646**, 414309 (2022)
Ren, Y., Li, Y., Li, W., Zhao, S., Chen, H., Liu, X.: High sensitivity and fast response infrared detector fabricated with the Bi_2Se_3–PbSe heterojunction. Appl. Surf. Sci. **584**, 152578 (2022)
Sajjad, M., Singh, N., Schwingenschlögl, U.: Strongly bound excitons in monolayer PtS_2 and $PtSe_2$. Appl. Phys. Lett. **112**(4), 043101 (2018)
Sharma, V., Okram, G. S., and Kuo, Y.-K. (2022). Metal to insulator transition, colossal Seebeck coefficient and large violation of Wiedemann–Franz law in nanoscale granular nickel. *Nanotechnology, 34*(3), 035702.
Sze, S.M., Li, Y., Ng, K.K.: Physics of Semiconductor Devices. Wiley (2021)
Tiwari, R.P., Kumar, V., Singh, S., Shah, J., Kotnala, R.K., Birajdar, B.: Structural phase transition, impedance spectroscopy and narrow optical band Gap in 1-x$KNbO_3$–x $BaSc_{1/2}Nb_{1/2}O_3$. J. Eur. Ceram. Soc. **38**(4), 1427–1433 (2018)
Virpal, Kumar, J., Thangaraj, R., Sharma, S., Singh, R.C.: Enhanced dielectric permittivity and photoluminescence in Cr doped ZnS nanoparticles. Appl. Surf. Sci. **416**, 296–301 (2017)
Wang, Y., Peng, X., Abelson, A., Xiao, P., Qian, C., Yu, L., et al.: Dynamic deformability of individual PbSe nanocrystals during superlattice phase transitions. Sci. Adv. **5**(6), 5eaaw5623 (2019)
Xu, Y., Kou, H., Fang, S., Wang, X., Bi, L.: Evaluation of potential reaction between $BaZr_{0.8}Y_{0.2}O_{3-\delta}$ ceramics and Pt at high temperatures. Ceram. Int. **45**(17A), 22383–22387 (2019)
Yan, S., Yang, Q., Feng, S., Shen, J., Yang, J., Tang, L., et al.: Effect of air atmosphere sensitization on formation of PbSe p–n junctions for high-performance photodetectors. J. Electron. Mater. **49**(8), 4929–4935 (2020)
Zeng, Q., Shi, J., Jiang, G., Yang, M., Wang, F., Chen, J.: Structures and optical absorptions of PbSe clusters from ab initio calculations. J. Chem. Phys. **139**(9), 094305 (2013)
Zimmermann, R., Rose, T., Crowe, T., & Grein, T.: An all-solid-state 1 THz radiometer for space applications. Paper presented at the Digest Sixth International Symposium on Space THz Technology, Pasadena (1995)